Flow of methane in shale nanopores at low and high pressure by molecular dynamics simulations

Zhehui Jin[1] and Abbas Firoozabadi[1,2,a)]
[1]*Reservoir Engineering Research Institute, Palo Alto, California 94301, USA*
[2]*Department of Chemical and Environmental Engineering, Yale University, New Haven, Connecticut 06511, USA*

(Received 8 April 2015; accepted 22 August 2015; published online 14 September 2015)

Flow in shale nanopores may be vastly different from that in the conventional permeable media. In large pores and fractures, flow is governed by viscosity and pressure-driven. Convection describes the process. Pores in some shale media are in nanometer range. At this scale, continuum flow mechanism may not apply. Knudsen diffusion and hydrodynamic expressions such as the Hagen-Poiseuille equation and their modifications have been used to compute flow in nanopores. Both approaches may have drawbacks and can significantly underestimate molecular flux in nanopores. In this work, we use the dual control volume-grand canonical molecular dynamics simulations to investigate methane flow in carbon nanopores at low and high pressure conditions. Our simulations reveal that methane flow in a slit pore width of 1–4 nm can be more than one order of magnitude greater than that from Knudsen diffusion at low pressure and the Hagen-Poiseuille equation at high pressure. Knudsen diffusion and Hagen-Poiseuille equations do not account for surface adsorption and mobility of the adsorbed molecules, and inhomogeneous fluid density distributions. Mobility of molecules in the adsorbed layers significantly increases molecular flux. Molecular velocity profiles in nanopores deviate significantly from the Navier-Stokes hydrodynamic predictions. Our molecular simulation results are in agreement with the enhanced flow measurements in carbon nanotubes. © *2015 AIP Publishing LLC.* [http://dx.doi.org/10.1063/1.4930006]

I. INTRODUCTION

Flow in shale media is a complex problem. In conventional permeable media, pores and fractures are large and pressure-driven convective flow (from viscosity) in the framework of continuum flow is applicable. Continuum flow can be described by Darcy's equation[1–3] and classical Navier-Stoke (NS) equations.[4] However, shale media have fine grains and pores may be in nanometer range. At this scale, fluid molecular distribution is inhomogeneous and surface adsorption may be significant.[5] Subsequently, Darcy's law and NS equations break down.[6] Majumder *et al.*[7] and Holt *et al.*[8] report that the flux in carbon nanotubes can be two to five orders of magnitude higher than the computed values from a conventional flow model. A number of modeling studies have indicated that molecular transport rates inside carbon nanotubes are orders of magnitude higher than in all other microporous materials, such as zeolite.[9–13] Knowledge in conventional flow is well advanced, but the mechanism of fluid flow in nanopores remains unclear.

Flow in nanopores can be in a variety of flow regimes.[14] The Knudsen number Kn[15] is used to classify the fluid flow regime. Kn is defined as the ratio of mean free path of fluid molecules λ to a characteristic dimension such as pore width W,

$$Kn = \frac{\lambda}{W}. \tag{1}$$

The mean free path of a molecule in an ideal gas is given by

$$\lambda = \frac{R_g T}{\sqrt{2}\pi\sigma^2 N_A P}, \tag{2}$$

in which R_g is the gas constant, T is temperature, σ is molecule diameter, N_A is the Avogadro number, and P is pressure. The mean free path is inversely proportional to pressure. If Knudsen number is sufficiently small, i.e., $Kn < 0.01$, fluid flow can be assumed as continuum and the NS or hydrodynamic Hagen-Poiseuille (HP) equations may describe flow with no-slip boundary conditions.[15] For a given fluid and nanopore system, a small Knudsen number indicates high system pressure. Assuming slit nanopores of width W, the HP equation for flux J^{HP} is given as

$$J^{HP} = -\frac{W^3}{12\eta}\left(\frac{\partial P}{\partial L}\right), \tag{3}$$

where η is viscosity. The measured water flow rate in carbon nanotubes reveals that flow enhancement can be three orders of magnitude greater than predictions from the HP equation.[8]

A. Slip effect

Flow enhancement in nanopores may be partly related to non-zero fluid velocity on the walls; fluid transport is subsequently enhanced over the predictions with the no-slip assumption.[1] Most authors use correction factors associated with the macroscopic transport to describe the slip effect. The so-called fluid slip can lead to higher apparent permeability for

a)Author to whom correspondence should be addressed. Electronic mail: abbas.firoozabadi@yale.edu

porous media.[16] The first attempt to account for the slip was by Klinkenberg in 1941.[17] He argued that in capillaries with a diameter comparable to the mean free path of gas molecules, interactions between the gas molecules and the capillary wall move the gas molecules forward in the direction of flow. The gas slippage reduces "viscous" drag and increases permeability.[18] The slip velocity depends on the permeating fluid, pore pressure, and size. The apparent permeability of porous media K_a based on the Klinkenberg effect is given as[17]

$$K_a = K_\infty \left(1 + \frac{b}{P_m}\right), \tag{4}$$

where K_∞ is the absolute permeability at high pressure when the Klinkenberg effect is negligible, b is the fluid slip factor,[1,19] and P_m the mean pore pressure. Klinkenberg effect is significant when the mean free path of fluid molecules approaches the pore size, i.e., when molecular collisions are significant with the pore wall rather than with other fluid molecules. Fluid permeability is then enhanced by "slip flow."

The slip effect can also be incorporated into the HP equation by using a theoretical dimensionless coefficient.[20] Assuming non-zero velocity U_w in the flow direction on the surface, the HP equation with slip velocity in slit geometry is given as

$$J^{HP} = -\frac{W^3}{12\eta}\left(\frac{\partial P}{\partial L}\right) + WU_w. \tag{5}$$

One way to account for U_w is by the slip length L_s,[21] defined as

$$L_s = -\frac{U_w}{\left(\frac{\partial U(z)}{\partial z}\right)_{z=W}}, \tag{6}$$

where U is velocity distribution in the flow direction. Slip length is the distance extrapolated into the surface to obtain vanishing velocity as assumed by no-slip boundary condition.[22] The derivative of U with respect to z on the surface is

$$\left(\frac{\partial U(z)}{\partial z}\right)_{z=W} = \frac{W}{2\eta}\frac{\partial P}{\partial L}. \tag{7}$$

The continuum flow with slip effect is given as (substituting Eqs. (6) and (7) into Eq. (5))

$$J^{HP} = -\frac{W^3}{12\eta}\left(\frac{\partial P}{\partial L}\right)\left(1 + \frac{6L_s}{W}\right). \tag{8}$$

When the slip length is much larger than the pore width, the continuum-based equations would not give accurate results.[8] The calculated slip length for water flow in carbon nanotubes can be as large as 1400 nm, which is almost three orders of magnitude larger than the pore width.[8]

Attempts to account for slip velocity in shale media include the works by Fathi *et al.*[16,23] who used the lattice Boltzmann method (LBM). LBM is employed to describe flow in nanopores by using macroscopic quantities (e.g., fluid velocity and density).[16,23] The fluid-wall interaction is taken into account through collisions with explicit intermolecular interactions between fluid molecules but surface atoms are neglected. Fathi *et al.*[16] ignored surface adsorption and assumed that after the collision with the wall, fluid molecules have non-zero velocity in the flow direction. They show that velocity at steady-state near the surface in capillaries can be twice of that in the middle of pores. As a result, the calculated permeability can be higher than that from the Klinkenberg effect. Later, these authors accounted for the effect of surface adsorption on flow by incorporating the LBM with the Langmuir slip model.[23] They used the equilibrium Langmuir isotherm as a function of local pore pressure to describe the slip velocity. Use of pressure (as a scalar quantity) may not be valid in small pores (e.g., less than few nm).[24] Fathi and Akkutlu[23] separated mass flux into the adsorbed and free mass fluxes. The adsorbed mass fluxes were defined assuming Fickian diffusion transport with arbitrary diffusion coefficients. LBM with the Langmuir slip model predicted that at high pressure the velocity distributions agree well with the Navier-Stokes flow and surface transport effect on molecular flow decreases with the pore size. LBM does not account for the inhomogeneous density distributions and may not be applicable for flow description in nanopores.

B. Knudsen diffusion

The transport of species in shale nanopores may be dominated by molecular diffusion. Many authors describe flow in shale nanopores by Knudsen diffusion plus the wall slip effect.[20] Knudsen diffusion is also combined with convection in the form of Klinkenberg correction factor for permeability.[25–27] Knudsen diffusion is based on the assumption that pore size is much smaller than the mean free path of molecules. Another assumption is that density of molecules in nanopores is low and fluid molecule-molecule collisions are negligible compared to fluid molecule-wall molecule collisions. After the collisions with the wall, fluid molecules reflect from the surface diffusely according to the cosine law: the probability of the outgoing direction is proportional to the cosine of the angle between this direction and normal vector.[28] Within the framework of Knudsen diffusion, fluid is assumed as ideal gas. The Knudsen flux J^K is given as

$$J^K = -\frac{D_k}{RT}\left(\frac{\partial P}{\partial L}\right), \tag{9}$$

where D_k is the Knudsen diffusivity. D_k is related to the pore width W and mean velocity of molecules $\bar{v}$,

$$D_k = \frac{W}{3}\bar{v} = \frac{W}{3}\sqrt{\frac{8R_gT}{\pi M}}, \tag{10}$$

where M is the molar mass. Note than in Eqs. (9) and (10) viscosity is absent; molecular flow is from diffusion. In shale subsurface formations, pressure is on the order of few hundred bar. At such high pressures, mean free path of a molecule is on the same order as the molecular size. Because of surface adsorption, fluid density is much higher than in an ideal gas. The inhomogeneous density distribution in nanopores[5] makes confined fluids very different from ideal gas. Holt *et al.*[8] report that the measured gas flow in carbon nanotubes of pore size of around 2 nm exceeds the flux from the Knudsen diffusion by at least one to two orders of magnitude.

C. Molecular simulation

Molecular simulation is a powerful tool to study transport in shale nanopores with inhomogeneous fluid density. The technique can also provide adsorption of various fluids on the surface.[24] Simultaneous modeling of adsorption and flow by the same model makes molecular simulations the ideal method to investigate flow in shale nanopores. There are a number of molecular simulation studies[1,4,10,29–39] of flow in nanopores. At low density, Bhatia *et al.* report that diffusion coefficient in silica nanopores is as much as one order of magnitude smaller than that from the Knudsen diffusion equation.[36,37] Krishna and van Baten[38,39] find that the Knudsen approach overpredicts the diffusivity compared to the MD simulation results in silica media. In a review article, Bhatia *et al.*[40] claim that due to significant adsorption, flow in silica nanopores is much lower than that from the Knudsen approach. They suggest that adsorption reduces the mobility of the fluid molecules. Zeolites and silicates have three-dimensional amorphous structures. Flow in these media may not fulfill the assumption of long nanopores in the Knudsen approach and hydrodynamic equations. Skoulidas *et al.*[10] report that the gas diffusivity in single-wall carbon nanotubes (SWNTs) can be orders of magnitude higher than that in zeolites. SWNTs have much smoother surfaces than zeolites. Some authors argue that the high transport rates in SWNTs is due to the very smooth internal surfaces, which give rise to near-specular reflection of molecules when they collide with the walls.[9,41] Specular reflection is the mirror-like reflection of molecules from a surface. Zeolites have rough surfaces which give more diffusive reflection from molecular collisions. There is no comparison of the measured fluxes to the results from the Knudsen diffusion and the HP equation. As a whole, the underlying mechanism of enhanced transport over conventional flow models in carbon nanotubes by Holt *et al.*[8] is still not clear.

The main goal of this work is to investigate methane transport in carbon nanotubes and provide an explanation for the enhanced transport reported by Holt *et al.*[8] In the past, flow enhancement has been contributed to the very smooth internal surfaces of carbon nanotubes and near-specular reflection of molecules.[9] In this work, we use the dual control volume-grand canonical molecular dynamics (DCV-GCMD)[1,29,31,42–45] to simulate flow in nanopores. We use a setting similar to Wang *et al.*[24,25] in our simulations.

DCV-GCMD implements two control volumes leading to the development of steady-state chemical potential difference to determine flow in nanopores.[42] A number of authors have used the DCV-GCMD simulations to investigate flow in nanopores. Cracknell *et al.*[29] show that methane velocity profile in carbon nanopores of 1 nm pore size is nearly parabolic with no significant slip. Their pore length is only 5 nm; the short length may significantly influence flow due to the correlation between two reservoirs. Firouzi and Wilcox[1] observe that molecular velocity on the surface is non-zero; in small carbon nanopores (1.14 nm pore width), the velocity on the surface is the same as that in the middle of the pore and in large pores (width larger than 7.6 nm); molecules have higher velocity in the middle than on the surface. They report high velocities in the range of 10^4 m/s. Firouzi and Wilcox[1] use pressure gradient to describe fluid flow. The pressure in slit-pores is inhomogeneous and cannot be interpreted by macroscopic pressure. These authors include both control volumes and flow regions in the slit-pore structures. Control volume in slit-pore structures may not be used to investigate non-equilibrium flow in nanopores between two bulk reservoirs. Wang *et al.*[30,31] use the DCV-GCMD to investigate transport of pure and binary gas mixtures in a carbon membrane in slit-like pores of finite length and width between two bulk reservoirs with different chemical potentials. All of these DCV-GCMD simulations[1,29–31,43,45] consider relatively short pore lengths (to 15 nm). When pore length is small, the end effect can significantly influence flow. Molecular simulations have not been conducted for high pressure gas flow in nanopores.

The remainder of this paper is organized as follows. In Section II, we present the molecular simulation method and define the molecular models used in this work. In Section III, we investigate methane flow in carbon nanopores in various pore widths and lengths connected to two bulk reservoirs at low and high pressures. We separate this section into two subsections: low pressure and high pressure flows. In Section IV, we present key conclusions.

II. SIMULATION MODEL

In our simulations, the slit nanopore is placed between two bulk reservoirs at two different pressures at constant temperature. Shale is composed of organic and inorganic

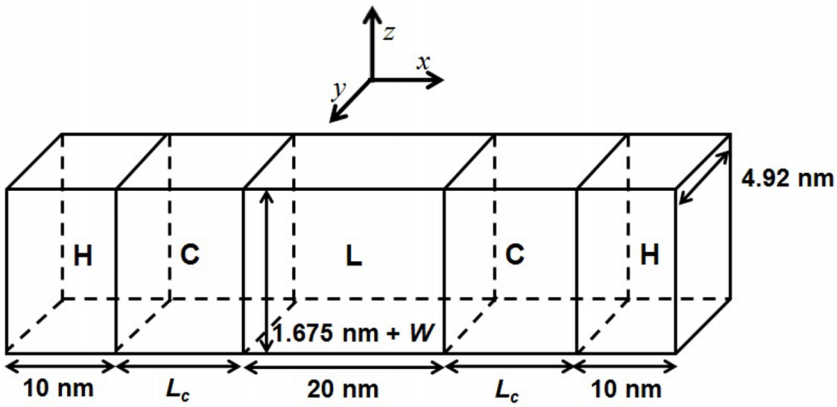

FIG. 1. Schematic representation of simulation box. The molecules flow along the $-x$ and $+x$ direction.

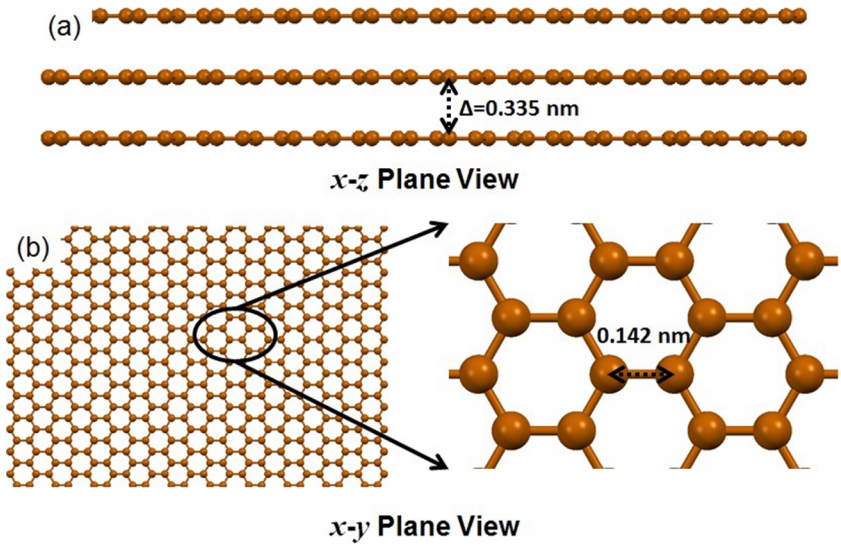

FIG. 2. Schematic representation of carbon sheet; (a) $x-z$ plane view; (b) $x-y$ plane view. Carbon atom size does not scale to LJ parameters.

materials. Organic materials which are mainly kerogen may have pores in nanometer range. Kerogen is hydrophobic and may be simulated by carbon materials.[5] We use full atomistic structure of graphite layers formed by carbon atoms to simulate nanopores. Both methane molecules and carbon atoms are modeled by the single-site Lennard-Jones (LJ) particles to describe the dispersion interactions. By incorporating these features, our DCV-GCMD provides the effect of pore structure on fluid flow in nanopores.

The simulation box consists of five regions as shown in Figure 1. The **H**, **L**, and **C** regions represent the high and low pressure control volumes, and carbon nanopores, respectively. We apply periodic boundary condition in all three directions except in **C** regions where it is applied in the y direction. Periodic boundary condition mimics a boundless wall. There are six graphite layers between the two slit pores. The **H** regions are placed at the two ends and the **L** region is placed in the middle of the box. The **C** regions are placed between the two control volumes. The sizes of **H** and **L** regions in the x direction are fixed at 20 nm. The carbon atoms are placed according to the structure of graphite layers[30,31] to construct the nanopores. We use three graphite layers to form one carbon sheet and two carbon sheets to set up the slit-like pores. The separation distance between the carbon atom centers in the two graphite layers is $\Delta = 0.335$ nm. The distance between two adjacent carbon atoms in the same graphite layer is 0.142 nm. The schematics of graphite layer and carbon sheet are shown in Figure 2. Carbon sheet positions are fixed throughout simulations. The box size is $(40 + 2 \times L_c)$ nm $\times 4.92$ nm $\times (1.675 + W)$ nm in the x, y, and z directions, respectively, where L_c is the length of nanopores and W is the pore width, which is the separation distance between the centers of carbon atoms of the two layers forming the slit pore. The length of nanopores in the y direction is the same as the box size (4.92 nm). The origin is set at the center of the simulation box.

TABLE I. LJ parameters of particles.

Particles	σ (nm)	ε/k_B (K)	Reference
CH_4	0.373	148.0	46
C	0.34	28.0	57

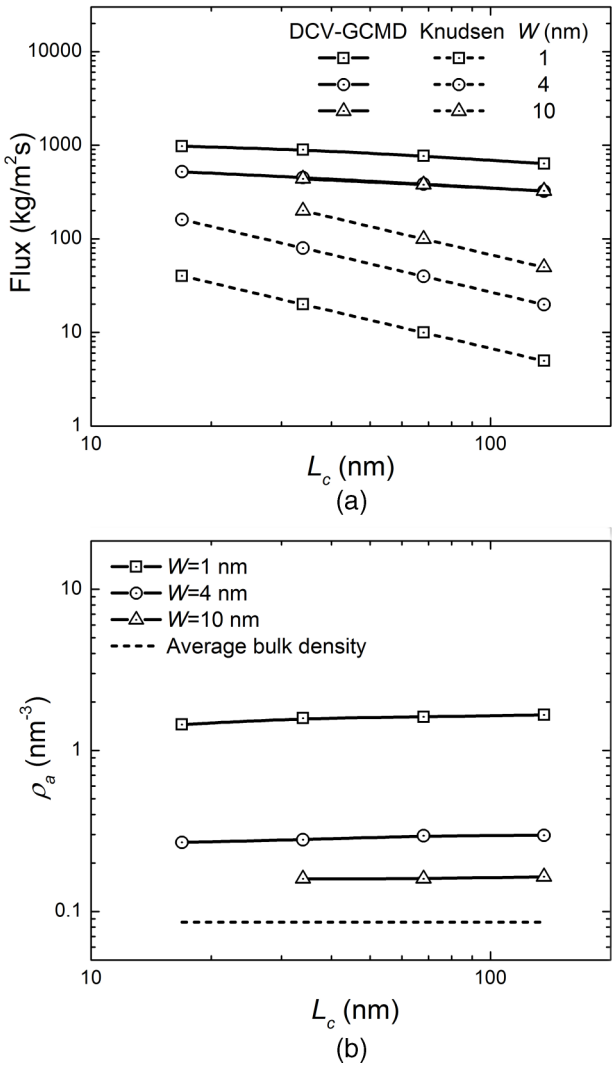

FIG. 3. (a) Methane molecular flux from DCV-GCMD and Knudsen diffusion; (b) average density in pores between control volume pressure $P_h = 6$ bars and $P_l = 1$ bar for the three nanopore widths versus length.

We use the TraPPE model[46] to simulate methane molecules. The interactions between methane and carbon atoms and between methane molecules are described by the pairwise-additive LJ 12-6 potentials,

$$u_{LJ}(r_{ij}) = 4\varepsilon_{ij}\left[\left(\frac{\sigma_{ij}}{r_{ij}}\right)^{12} - \left(\frac{\sigma_{ij}}{r_{ij}}\right)^{6}\right], \tag{11}$$

where r_{ij}, ε_{ij}, and σ_{ij} are the separation, LJ well depth, and LJ size, respectively. Unlike interactions are computed using the standard Lorentz-Berthelot combining rules

$$\sigma_{ij} = (\sigma_{ii} + \sigma_{jj})/2, \tag{12}$$

$$\varepsilon_{ij} = \sqrt{\varepsilon_{ii}\varepsilon_{jj}}. \tag{13}$$

The size parameter σ and energy parameter ε for methane and carbon atoms are listed in Table I. All of the LJ interactions are truncated at a distance of 1.07 nm. The interaction between a methane molecule and carbon atoms is obtained by summing over all carbon atoms in the nanopores.

A. Dual control volume-grand canonical molecular dynamics

The DCV-GCMD method has been used to study chemical potential-driven flow through membranes[30,31] and slit nanopores.[1,29] The method combines the MD moves in the entire system with the grand canonical Monte Carlo (GCMC) particle insertions and removals in the two control volumes (CVs). In our work, MD and GCMC moves are applied to methane molecules.

Throughout the simulation volume, standard MD simulation moves are employed. The equations of motion are solved by the Verlet velocity algorithm[47] using the Berendsen thermostat[48] to maintain constant temperature. Linked cells[49] are employed to reduce the computation time. The chemical potential of methane in the CVs is kept constant using a sufficient number of GCMC insertions and removals.[42,43,50] The probability of inserting a methane molecule p^+ is given by

$$p^+ = \min\left\{\frac{ZV_{CV}}{N_{CV}+1}\exp\left(-\frac{\Delta U}{k_BT}\right), 1\right\}, \tag{14}$$

where $Z = \exp(\mu/k_BT)/\Lambda^3$ is the absolute activity at temperature T, Λ is the de Broglie wavelength, μ is the chemical potential, k_B is the Boltzmann's constant, ΔU is the potential energy change from inserting or removing a molecule, V_{CV} is the volume of CV, and N_{CV} is the number of methane molecules in each CV. As particles are inserted, the Maxwell-Boltzmann distribution[51] is used to assign velocities.

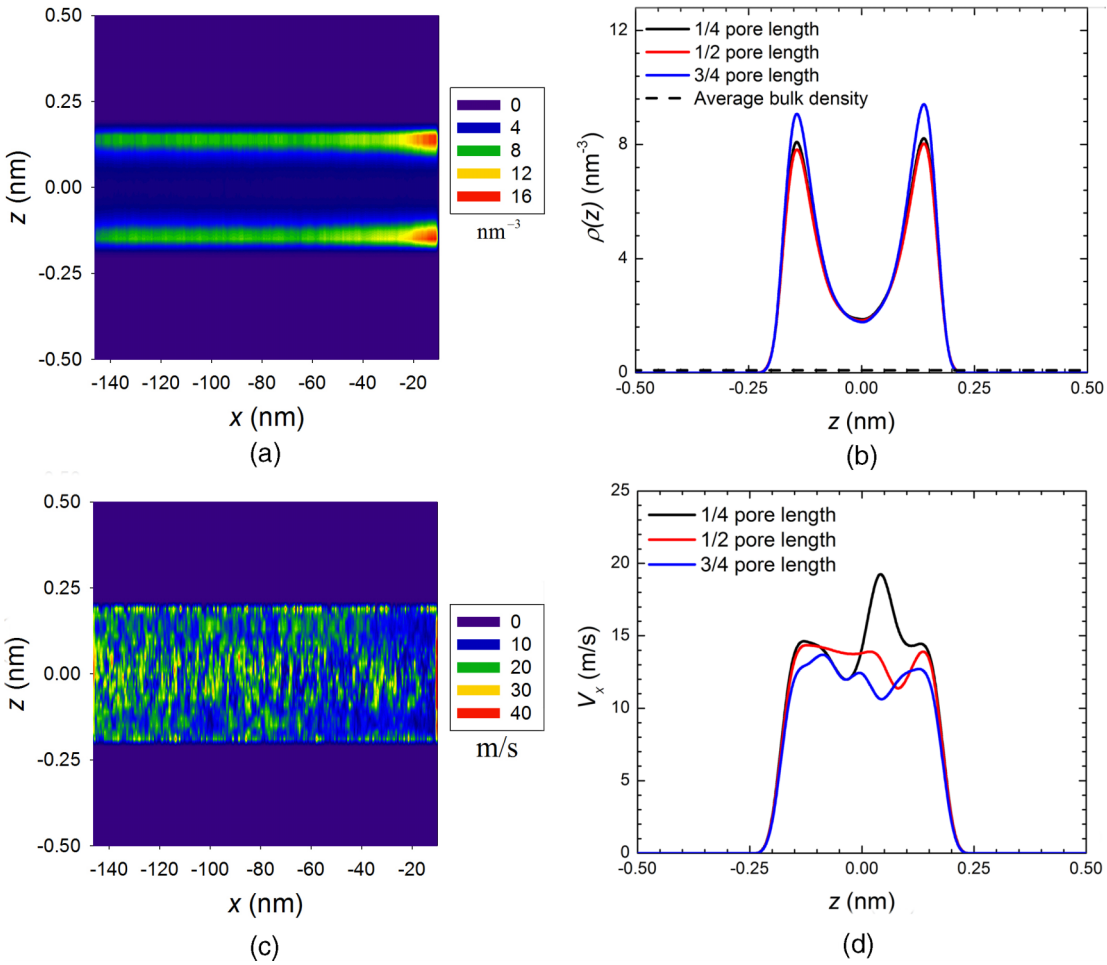

FIG. 4. (a) $x-z$ plot of density distributions; (b) density profiles at the 1/4, 1/2, 3/4 pore length in nanopores between control volume pressure $P_h = 6$ bars and $P_l = 1$ bar. Average bulk density is also shown in (b). (c) $x-z$ plot of velocity distributions; (d) velocity profiles at the 1/4, 1/2, 3/4 pore length: $W = 1$ nm and $L_c = 136.178$ nm.

The probability of removing a molecule p^- is given by

$$p^- = \min\left\{\frac{N_{CV}}{ZV_{CV}}\exp\left(-\frac{\Delta U}{k_BT}\right), 1\right\}. \quad (15)$$

Ten GCMC moves in each CV are followed by one MD integration step.[1] After particle insertion/removal, we use the Verlet velocity algorithm to calculate forces acting on the molecules. Insertion/removal of a particle disturbs the system, especially in the force calculation. Early in the work, we used the more sophisticated Beeman's algorithm[52] in the solution of the equation of motion. The method uses forces on the atoms at previous and current time steps. Due to disturbance by insertion/removal, Beeman's algorithm breaks down and we obtained incorrect flux and density distribution in the nanopores.

The chemical potentials are obtained from Widom's particle insertion method[53] in the independent *NVT* Monte Carlo simulations of bulk methane fluid. The time step of MD simulation is $\Delta t = 2$ fs. We use 10-ns simulation time for the system to reach steady state and 10-ns simulation time to calculate density, velocity profiles, and fluxes. In order to have de-correlated sampling,[54] we sample the system every 20 fs. The system temperature is fixed at 298.15 K.

The flux of molecules J_x in the x direction is computed counting the net number of methane molecules crossing halfway along each nanopore region,[42,55]

$$J_x = \frac{n^{hl} - n^{lh}}{n_t \Delta t A_{yz}}, \quad (16)$$

where n^{hl} and n^{lh} are the number of molecules moving from high to low pressure region and vice versa, n_t is the number of time steps of sampling, A_{yz} is the cross-section area of carbon nanopore. The final estimate of the flux is the average of the flux in the two nanopore regions.

III. RESULTS AND DISCUSSIONS

In this section, we present the flux, density distributions and profiles, and velocity distributions and profiles of methane molecules in different pore widths and pressures of the bulk control volumes at low and high pressure flows.

A. Low pressure flow

In Figure 3(a), we present methane molecular flux from pressure $P_h = 6$ bars to $P_l = 1$ bar in the two control volumes for different pore widths and lengths. For comparison, we also show the predictions from the Knudsen flow. We assume linear pressure drop in the Knudsen diffusion of Eq. (9),

$$J^K = -\frac{D_k}{RT}\frac{P_l - P_h}{L_c}. \quad (17)$$

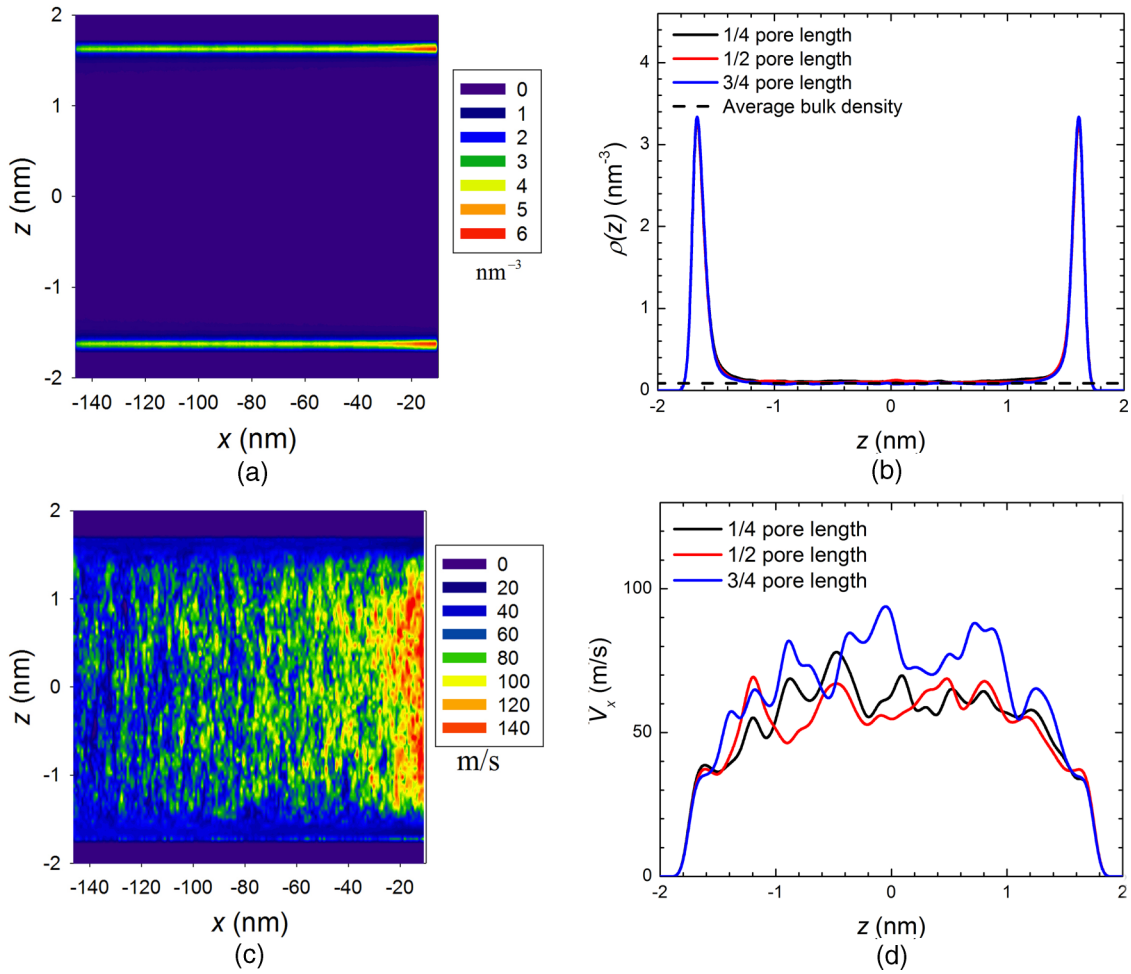

FIG. 5. The same as Figure 4 but for control volume pressures $P_h = 6$ bars and $P_l = 1$ bar: $W = 4$ nm and $L_c = 136.178$ nm.

The flux from the DCV-GCMD simulations is higher than that from the Knudsen diffusion. We do not show the results in short slit pores. When the pore length is short, the molecular mean free path is comparable to or even larger than the nanopore length and then, Knudsen diffusion may not be applicable. In addition, when pore size is comparable to length, the end effect may become significant. In small pores ($W = 1$ nm), the molecular flux is one to two orders of magnitude larger than the Knudsen diffusion. Our calculations reveal that at low pressure conditions, flux decreases with pore width and length. As pore width increases, the contribution from the surface adsorption decreases and fewer molecules are adsorbed on the nanopore surfaces. We also plot the average fluid density inside the nanopore, ρ_a in Figure 3(b), which is given by

$$\rho_a = \frac{\langle N_c \rangle}{V_c}, \tag{18}$$

where $\langle N_c \rangle$ is the ensemble average number of molecules in the nanopores and $V_c = L_c \times 4.92 \times W$ nm^3 is the pore volume. For comparison, we also present the average bulk density ρ_a^b based on the inlet and outlet reservoirs,

$$\rho_a^b = \frac{1}{2}\left(\rho_h^b + \rho_l^b\right), \tag{19}$$

in which, ρ_h^b and ρ_l^b are bulk density at the inlet and outlet reservoirs, respectively. As Figure 3(b) shows, the average density in nanopores of $W = 1$ nm is around $20\rho_a^b$. With increase in pore width, ρ_a decreases due to lower adsorption. On the other hand, the Knudsen diffusion coefficient increases with pore width. One to two orders of magnitude higher flux than the Knudsen diffusion is due to flow of the adsorbed layer and inhomogeneous distributions of methane molecules. Ideal gas assumption is not valid in nanopores even at low pressures. Pressure is a tensor and non-uniform inside the nanopores, which is very different from that in the bulk reservoir. Knudsen diffusion is based on ideal gas assumption and linear pressure gradient which may not be applicable in small pores. Bhatia *et al.*[9] point out that in a smooth carbon nanotube, the molecule-wall collisions may be a combination of specular and diffuse collisions, leading to faster molecular transport.[8] In the following, we investigate density and velocity profiles in three different pore widths.

***W* = 1 nm**: In Figure 4(a), we present the $x - z$ plot of density distribution of methane molecules in nanopores of $W = 1$ nm and $L_c = 136.178$ nm. Due to symmetry, we present results of the left carbon nanopore with the higher pressure reservoir as inlet and the lower pressure reservoir as outlet. Methane molecules form adsorption layers throughout the pores. Interestingly, density of the adsorption layer increases as approaching the outlet. We also present density profiles in the pore at the 1/4, 1/2, and 3/4 cross sections in Figure 4(b). The bulk average density profiles are also shown in the

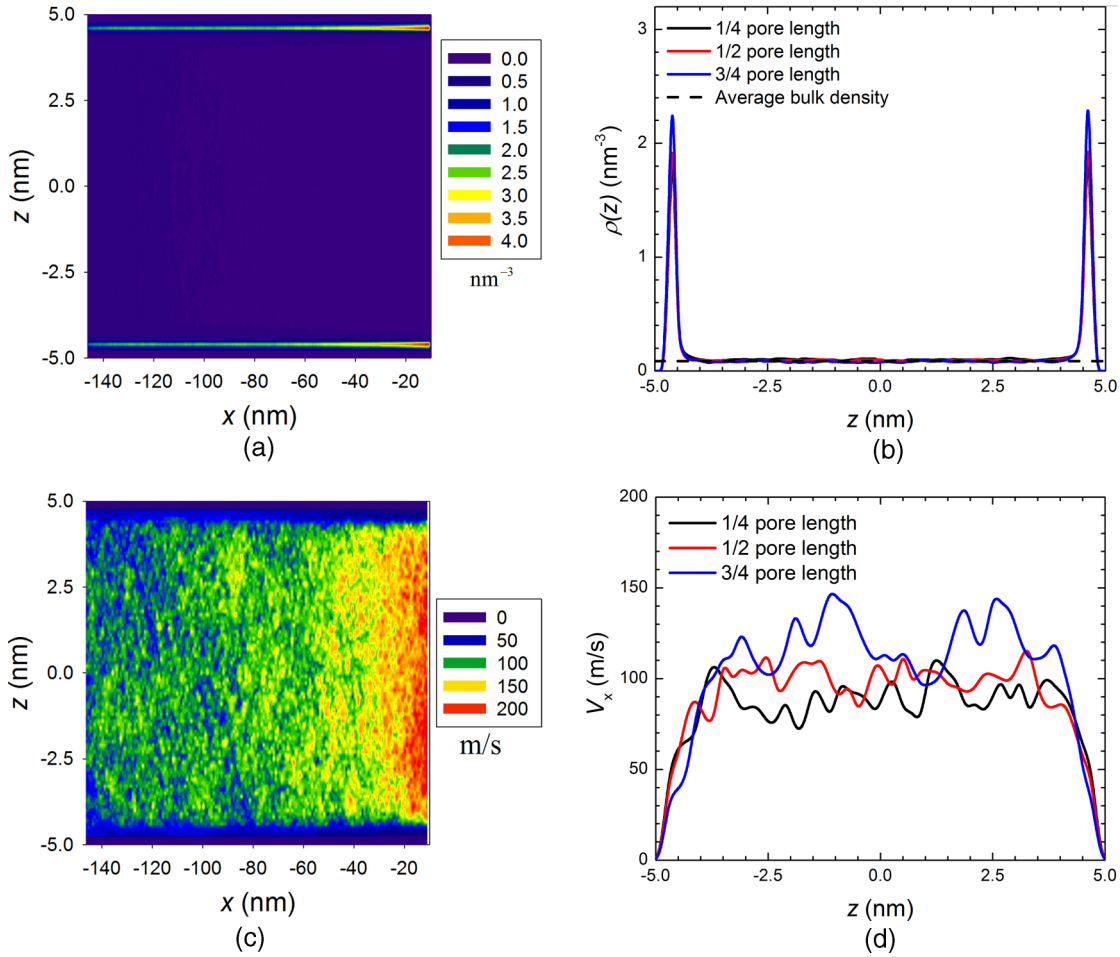

FIG. 6. The same as Figure 4 but for control volume pressures $P_h = 6$ bars and $P_l = 1$ bar: $W = 10$ nm and $L_c = 136.178$ nm.

same figure. Due to high surface adsorption, the density in nanopores is much higher than the average bulk density. Note that the density in the adsorption layer increases slightly as approaching the outlet due to higher mobility of the molecules in the flow direction at the inlet. The molecules in the adsorption layer move along the pores rather than being fixed at the adsorption sites. We present the corresponding $x-z$ plot of velocity distributions in the x direction in Figure 4(c). In nanopores, fluid-surface interactions influence the velocity profile.[1] The main contribution to flux in narrow nanopores is from the mobility of adsorption layers. Because Knudsen diffusion ignores surface adsorption and inhomogeneity in the pores, it significantly underestimates molecular flux. On the other hand, GCMD explicitly considers intermolecular interactions and takes into account the inhomogeneity and surface adsorption. We also present velocity profiles in the x direction at the 1/4, 1/2, and 3/4 cross sections in Figure 4(d). The velocity profile shows non-parabolic behavior along the z direction. The non-symmetric shape is due to small number of molecules in the middle of the pore.

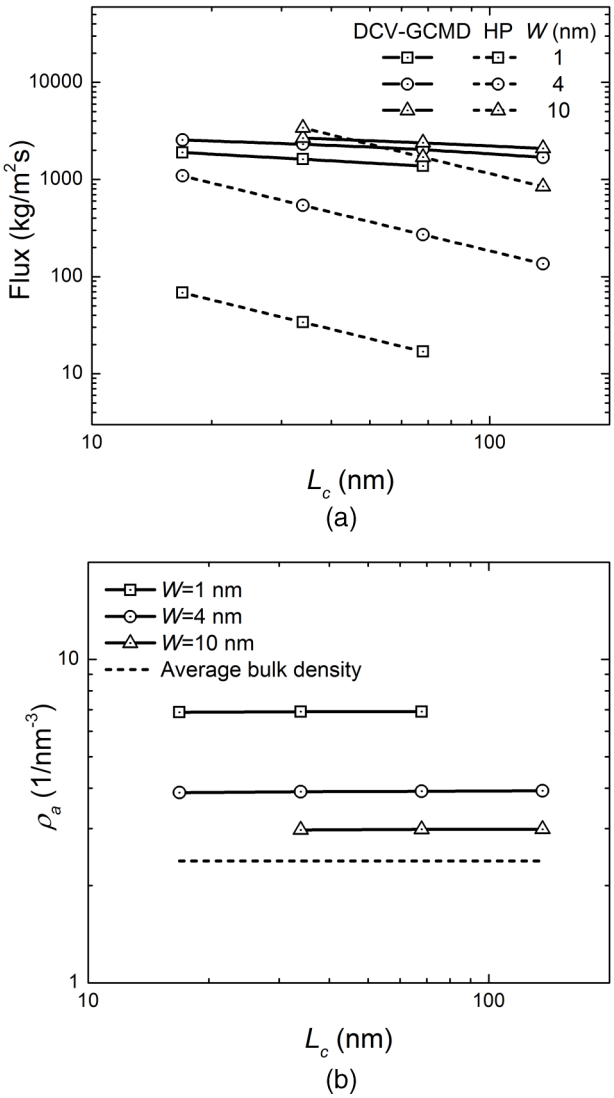

FIG. 7. (a) Methane molecular flux from DCV-GCMD and HP expression; (b) average density in pores between control volume pressure $P_h = 100$ bars and $P_l = 70$ bars for the three nanopore widths versus length.

$W = 4$ nm: In Figure 5(a), we present the $x-z$ plot of density distribution of methane molecules in $W = 4$ nm and $L_c = 136.178$ nm pores. Similar to Figure 4(a), methane molecules form adsorption layers throughout the pores. The adsorption layer density is less than that in small nanopores ($W = 1$ nm). Similar to $W = 1$ nm, density in the adsorption layer increases as approaching the outlet due to mobility of adsorption layer. We present the density profiles at the 1/4, 1/2, and 3/4 cross sections in Figure 5(b). The disparity between nanopore average fluid density and bulk density in $W = 4$ nm is less than that in $W = 1$ nm nanopores. In the middle of the pore, the density distribution is close to average bulk density. The corresponding $x-z$ plot of velocity distribution in the x direction is presented in Figure 5(c). The velocity on the surface is non-zero and molecular velocity is faster than that in small nanopores ($W = 1$ nm). The velocity in the middle of the pore is higher than that of adsorption layer. We present velocity profiles along the z direction at the 1/4, 1/2, and 3/4 cross sections in Figure 5(d). Molecular flux is dependent on the density distributions and molecular velocity distributions. The velocity of adsorption layer is smaller than that in the middle of the pore. But due to much higher density, adsorption layer with non-zero velocity is the main contribution to flow in nanopores.

$W = 10$ nm: The $x-z$ plot of density distribution of methane molecules in nanopores of $W = 10$ nm and $L_c = 136.178$ nm pores is shown in Figure 6(a). The adsorption layer is observed throughout the nanopores. However, in contrast to $W = 1$ nm and $W = 4$ nm, the strength of adsorption layer is weaker. When the pore width is large ($W = 10$ nm), the effect of surface adsorption may become less pronounced as shown in the density profiles at the 1/4, 1/2, and 3/4 cross sections in Figure 6(b). Density profile in the middle of the pore is close to the average bulk density. We present the $x-z$ plot of velocity distribution in the x direction in nanopores of $W = 10$ nm and $L_c = 136.178$ nm in Figure 6(c). Molecular velocity is higher than that in the smaller pores ($W = 1$ nm and $W = 4$ nm). The coupling of velocity and surface adsorption does appreciably affect the velocity. The velocity profiles at the 1/4, 1/2, and 3/4 cross sections in Figure 6(d) indicate that velocity on the surface is non-zero and lower than the velocity in the middle of the pore. Comparing to $W = 4$ nm, density in the adsorption layer decreases but molecular velocity increases. As a result, due to the coupling of density and velocity profile, fluxes of $W = 4$ nm and $W = 10$ nm are similar as shown in Figure 3(a).

B. High pressure flow

In Figure 7(a), we present the methane molecular flux between the control volumes at pressure $P_h = 100$ bars and

TABLE II. Slip lengths of HP equation in high pressure flow.

W (nm)	L_c (nm)	Flux (GCMD) (kg/m² s)	Flux (HP) (kg/m² s)	L_s (nm)
1	68.018	1374.87	16.94	13.36
4	136.178	1690.68	135.41	7.66

at $P_l = 70$ bars in various pore widths and lengths from DCV-GCMD simulations and the HP expression. Assuming linear pressure dependency between the inlet and outlet in the HP expression, one can write

$$J^{HP} = -\frac{W^3}{12\eta}\frac{P_l - P_h}{L_c}. \quad (20)$$

We use the mean viscosity of bulk fluids at P_h and P_l. The data are from the National Institute of Standards and Technology (NIST) Chemistry WebBook. In small pores ($W = 1$ nm), methane flow from DCV-GCMD simulations can be more than two orders of magnitude larger than that from the HP expression; in large pores ($W = 10$ nm), methane flow from DCV-GCMD simulations is smaller than that from the HP equation when the length is short; as pore length increases, molecular flow is higher than that from the HP equation and enhancement increases. Whitby *et al.*[56] have reported that the measured flow in carbon nanopores with large inner diameters (44 nm) can be one order of magnitude larger than the HP expression. The HP expression has a flux dependency of W^3; DCV-GCMD simulations predict that flow increases with pore width moderately. In small nanopores ($W = 1$ nm), methane molecules pack the surface and reduce overall mobility. As pore width increases, molecular velocity increases. At high pressure, difference in the adsorption layer and the rest of the pore for various pore widths is less pronounced than at low pressure. The calculated slip lengths L_s, for different pore widths and lengths are given in Table II. L_s for $W = 1$ nm is one order of magnitude larger than the pore width suggesting that the slip-flow mechanism may not be applicable to high pressure flow in 1 nm nanopores. We present the average density in nanopores ρ_a from Eq. (18) in Figure 7(b). In contrast to low pressure, the difference between ρ_a in small nanopores ($W = 1$ nm) and bulk average density ρ_a^b is less drastic. Increase in flux with pore width may be due to increased velocity in larger nanopores as we will discuss later. The HP equation does not include the effect of surface adsorption and inhomogeneous density distributions in nanopores and assumes that velocity on the surface is zero.

We present the $x - z$ plots of density distributions and profiles, and velocity distributions and profiles in the x direction for methane molecules in nanopores of three different pore widths versus length in the following.

$W = 1$ nm: We first present the density distributions of $W = 1$ nm and $L_c = 68.018$ nm in Figure 8(a). Methane molecules form adsorption layers throughout the nanopores. Mobility of the molecules on the surface is the main reason that molecular flux is much higher than that from the HP expression. In contrast to low pressure flow, the density in the

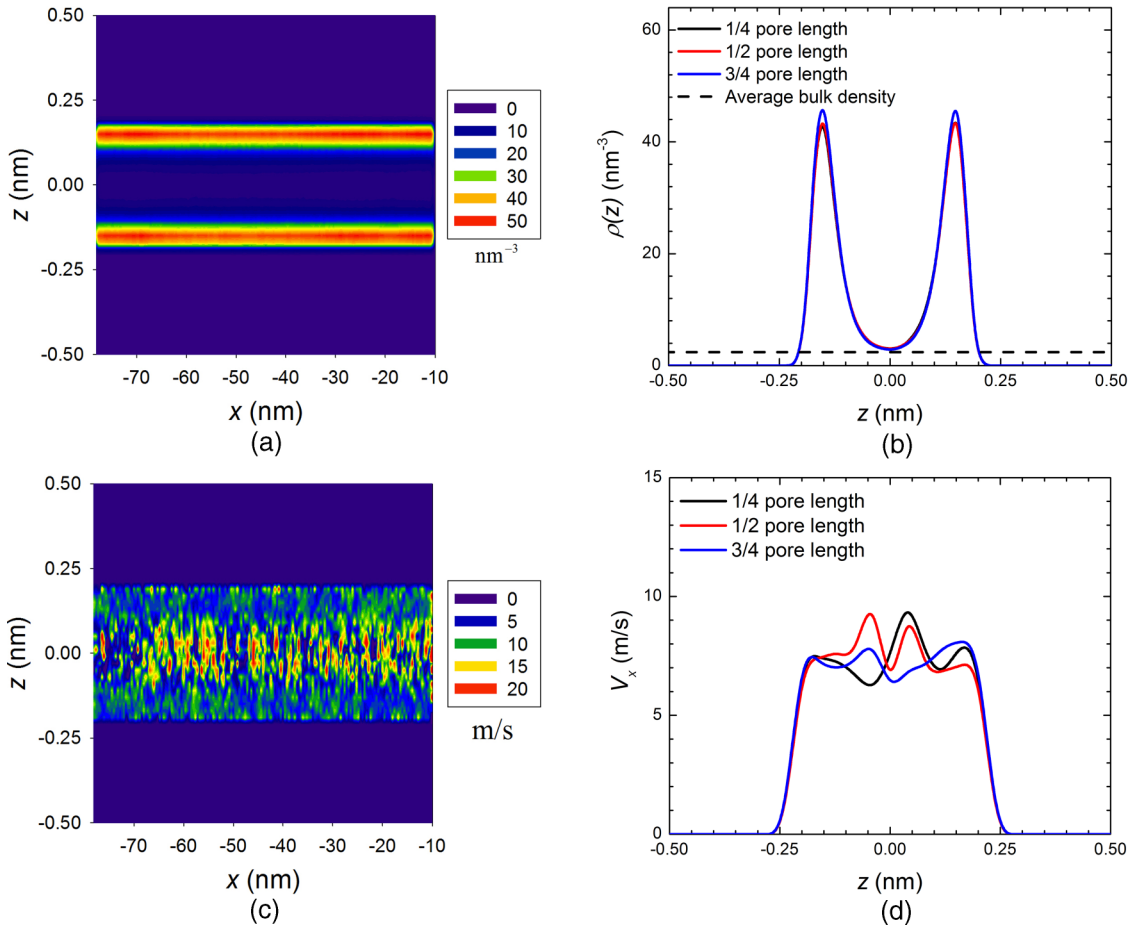

FIG. 8. (a) $x - z$ plot of density distributions; (b) density profiles at the 1/4, 1/2, 3/4 pore length in nanopores between control volume pressure $P_h = 100$ bars and $P_l = 70$ bars. Average bulk density is also shown in (b). (c) $x - z$ plot of velocity distributions; (d) velocity profiles at the 1/4, 1/2, 3/4 pore length: $W = 1$ nm and $L_c = 68.018$ nm.

adsorption layer does not show variation in the x direction. We also present the density profiles at the 1/4, 1/2, and 3/4 cross sections and average bulk density in Figure 8(b). The density profile in nanopores is enhanced over average bulk density but the difference in the density profiles at different positions of the pores is negligible. Velocity in the flow direction is greatly reduced due to higher molecular density distributions in nanopores comparing to the low pressure flow. The velocity distribution in the x direction is shown in Figure 8(c). Similar to low pressure flow, the velocity on the surface is non-zero. The velocity profiles at the 1/4, 1/2, and 3/4 cross sections are depicted in Figure 8(d). As in the low pressure conditions, the velocity profile is non-parabolic. Because velocity on the surface is comparable to the middle of the nanopores, mobility of the adsorbed molecules is the main contribution to molecular flux in small nanopores ($W = 1$ nm).

***W* = 4 nm**: We present the $x - z$ plot of density distributions of methane molecules in nanopores of $W = 4$ nm and $L_c = 136.178$ nm in Figure 9(a). Methane molecules form adsorption layers throughout the nanopores. As expected, the adsorption layer in $W = 1$ nm is stronger than that in $W = 4$ nm. The density profiles at the 1/4, 1/2, and 3/4 cross sections are shown in Figure 9(b). Note the formation of a second adsorption layer. There is very little difference between the adsorption layers in different cross sections. The velocity distribution in the x direction is presented in Figure 9(c). Velocity on the surface is comparable to that in the middle of the pores at the 1/4, 1/2, and 3/4 cross sections as shown in Figure 9(d). Molecular velocity is faster than that in the smaller pores ($W = 1$ nm). Because of reduced correlation in adsorption layers and the rest of the pores as the width increases, molecular flux increases with pore width.

***W* = 10 nm**: Contribution from mobility of adsorbed molecules is greatly reduced in large nanopores as shown in the $x - z$ plot of density profile in $W = 10$ nm and $L_c = 136.178$ nm in Figure 10(a). Methane molecules form adsorption layer throughout the nanopores. However, there is significant reduction in the adsorption strength in $W = 10$ nm compared to smaller pores ($W = 1$ nm and $W = 4$ nm). As a result, in large nanopores ($W = 10$ nm), the contribution from surface adsorption to molecular flux is less significant. The density profiles at the 1/4, 1/2, and 3/4 cross sections are shown in Figure 10(b). Density in the middle section of the pores is close to average bulk density. We also present the $x - z$ plot of the velocity distribution in the x direction in Figure 10(c). As pore width increases, molecular velocity further increases. We present the velocity profile at the 1/4, 1/2, and 3/4 cross sections in Figure 10(d); molecular velocity in the middle of the pore is higher than that on the surface. The increase in flux with pore width is due to enhanced molecular velocities, while the effect of pore size on density distribution is less significant.

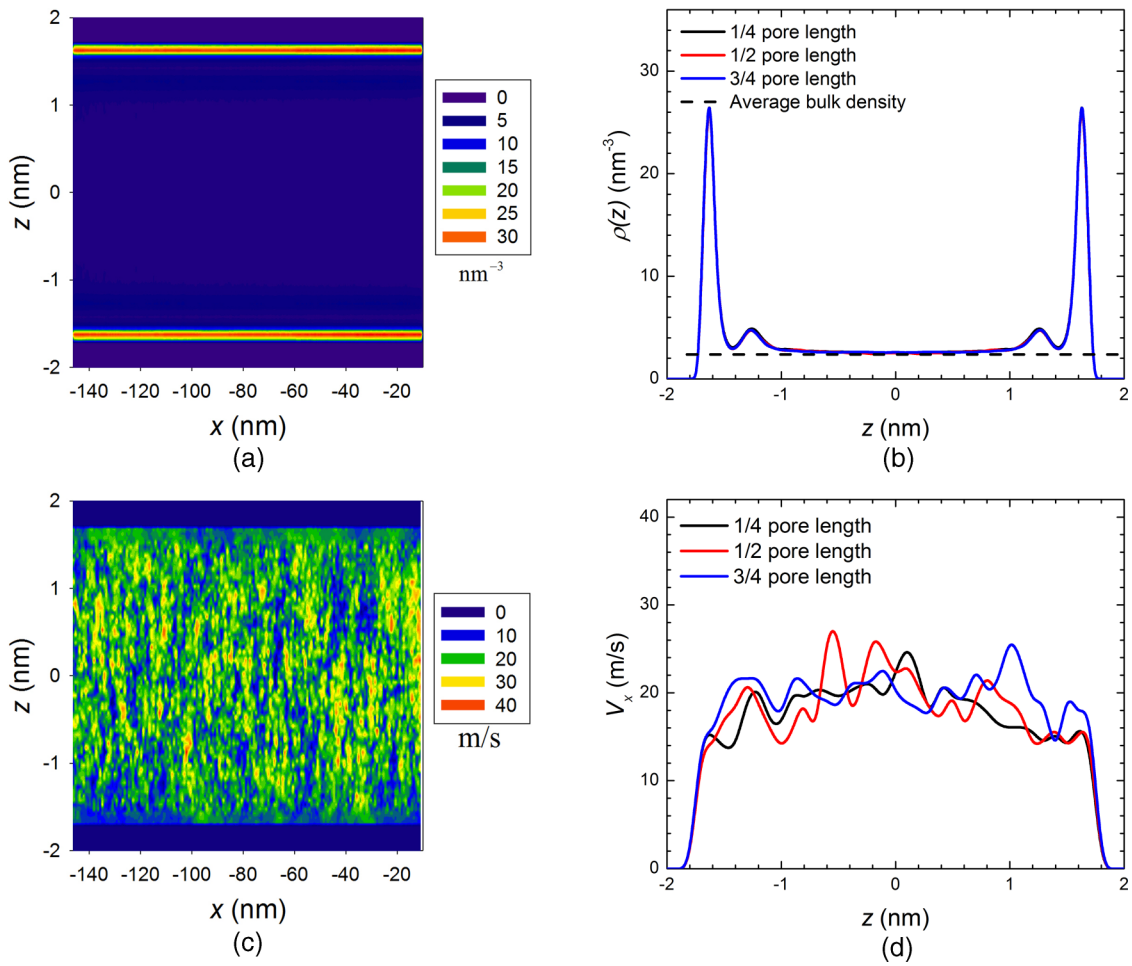

FIG. 9. The same as Figure 8 but for control volume pressure $P_h = 100$ bars and $P_l = 70$ bars: $W = 4$ nm and $L_c = 136.178$ nm.

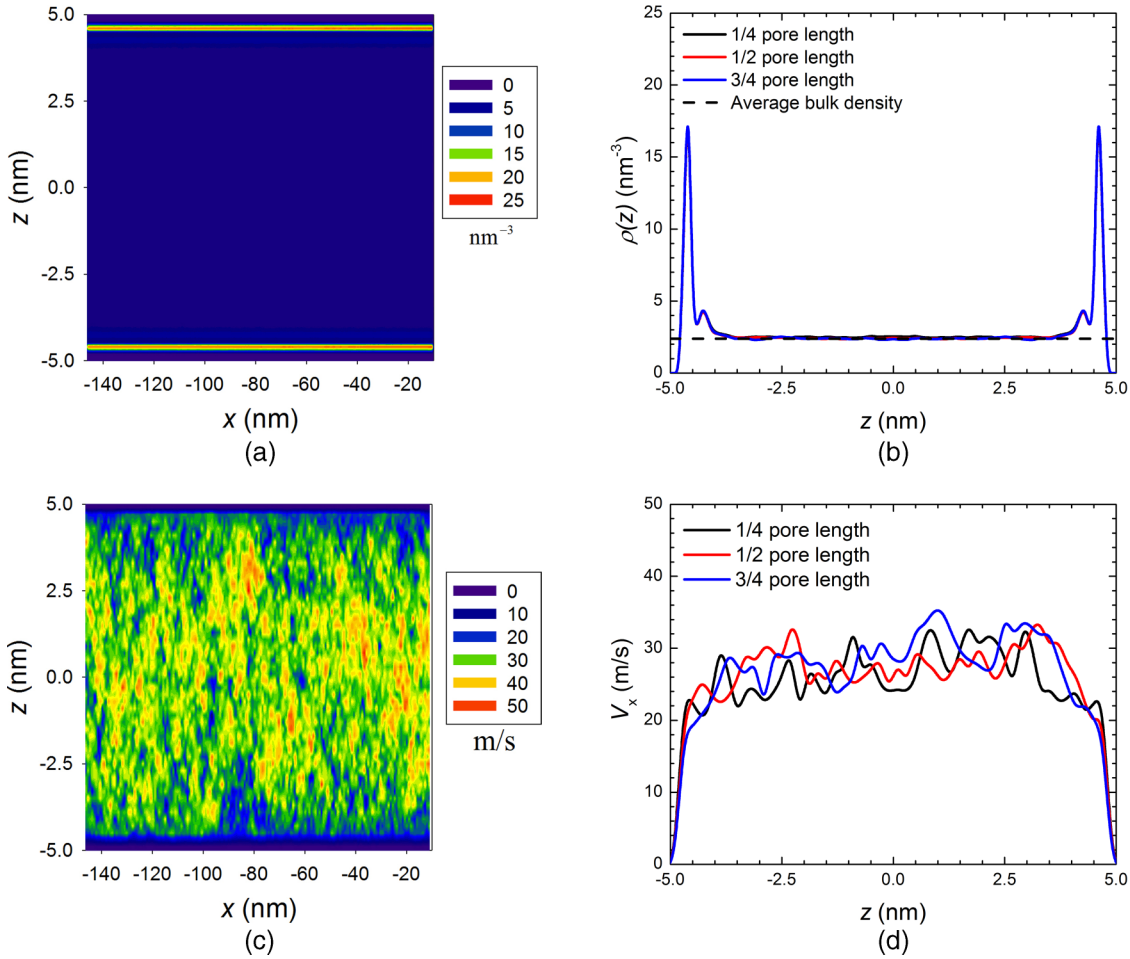

FIG. 10. The same as Figure 8 but for control volume pressure $P_h = 100$ bars and $P_l = 70$ bars: $W = 10$ nm and $L_c = 136.178$ nm.

IV. CONCLUSIONS

Our molecular dynamics simulations demonstrate that the contribution from the mobility of adsorbed molecules has significant effects on flow enhancement in methane flux both at low and high pressures in small nanopores. The results are in agreement with methane flux measurements in small nanopores by Holt *et al.*[8] The data from these authors reveal one to two orders of magnitude flux enhancement in 2-nm pores compared to the Knudsen diffusion. In a pore size of 15-nm there is much less enhancement. As pointed out in this work, fluid homogeneity and concept of pressure driven flow, which are central to the hydrodynamic flow and the Knudsen diffusion, are not in line with the flow of inhomogeneous fluid density in small nanopores.

For low pressure flow, the mobility of molecules in adsorption layers and high local fluid density distribution significantly increases methane flux. As a result, the flux can be one to two orders of magnitude larger than predictions from the Knudsen diffusion for long carbon nanopores of small size ($W = 1$ nm). Knudsen diffusion is based on the homogeneous density and ideal gas assumption ignoring surface adsorption. Methane molecular velocity increases with pore width, but flux has the opposite trend because of the effect of high local density distribution.

For high pressure flow, flux increases moderately with pore width. The HP equation, however, underestimates flux in small nanopores significantly due to neglect of the adsorption layer and its mobility. When the pore length is small there may be end effects at the inlet and outlet; the results from the hydrodynamic expression may not be applicable. As pore width increases, molecular velocity increases. The increased velocity contributes to flux increases with pore width. For a small pore width ($W = 1$ nm), flux can be one order of magnitude larger than that from the HP equation. The HP equation ignores surface adsorption and assumes that velocity on the surface is zero.

In this work, the full effect of length has not been investigated due to limitations in computational power. In the future, we plan to investigate liquid flow in nanopores as well as length effects.

ACKNOWLEDGMENTS

This work was supported by member companies of the Reservoir Engineering Research Institute. Their support is greatly appreciated.

[1]M. Firouzi and J. Wilcox, J. Chem. Phys. **138**, 064705 (2013).
[2]S. P. Neuman, Acta Mech. **25**, 153–170 (1977).
[3]S. Whitaker, Transp. Porous Media **1**, 3–25 (1986).
[4]K. P. Travis, B. D. Todd, and D. J. Evans, Phys. Rev. E **55**, 4288–4295 (1997).
[5]Z. Li, Z. Jin, and A. Firoozabadi, SPE J. **19**, 1096–1109 (2014).
[6]I. Bitsanis, T. K. Vanderlick, M. Tirrell, and H. T. Davis, J. Chem. Phys. **89**, 3152–3162 (1988).

[7]M. Majumder, N. Chopra, R. Andrews, and B. J. Hinds, Nature **438**, 44 (2005).
[8]J. K. Holt, H. G. Park, Y. Wang, M. Stadermann, A. B. Artyukhin, C. P. Grigoropoulos, A. Noy, and O. Bakajin, Science **312**, 1034–1037 (2006).
[9]S. K. Bhatia, H. Chen, and D. S. Sholl, Mol. Simul. **31**, 643–649 (2005).
[10]A. I. Skoulidas, D. M. Ackerman, J. K. Johnson, and D. S. Sholl, Phys. Rev. Lett. **89**, 185901 (2002).
[11]D. M. Ackerman, A. I. Skoulidas, D. S. Sholl, and J. Karl Johnson, Mol. Simul. **29**, 677–684 (2003).
[12]H. Chen and D. S. Sholl, J. Am. Chem. Soc. **126**, 7778–7779 (2004).
[13]V. P. Sokhan, D. Nicholson, and N. Quirke, J. Chem. Phys. **117**, 8531–8539 (2002).
[14]S. Kandlikar, S. Garimella, D. Li, S. Colin, and M. R. King, *Heat Transfer and Fluid Flow in Minichannels and Microchannels* (Elsevier, London, 2005).
[15]E. Roohi and M. Darbandi, Phys. Fluids **21**, 082001 (2009).
[16]E. Fathi, A. Tinni, and I. Y. Akkutlu, Int. J. Coal Geol. **103**, 51–59 (2012).
[17]L. J. Klinkenberg, "The permeability of porous media to liquids and gases," in *Drilling and Production Practice* (American Petroleum Institute, 1941).
[18]C. A. McPhee and K. G. Arthur, "Klinkenberg permeability measurements: Problems and practical solutions," in *Advances in Core Evaluation II: Reservoir Appraisal: Reviewed Proceedings of the Second Society of Core Analysts European Core Analysis Symposium*, *20-22 May 1991* (CRC Press, London, UK, 1991), p. 371.
[19]Y.-S. Wu, K. Pruess, and P. Persoff, Transp. Porous Media **32**, 117–137 (1998).
[20]F. Javadpour, J. Can. Pet. Technol. **48**, 16–21 (2009), PETSOC-09-08-16-DA.
[21]E. M. Kotsalis, J. H. Walther, and P. Koumoutsakos, Int. J. Multiphase Flow **30**, 995–1010 (2004).
[22]C. Cottin-Bizonne, J.-L. Barrat, L. Bocquet, and E. Charlaix, Nat. Mater. **2**, 237–240 (2003).
[23]E. Fathi and I. Y. Akkutlu, SPE J. **18**, 27–37 (2012).
[24]Z. Jin and A. Firoozabadi, "Thermodynamic modeling of phase behavior in shale media," SPE J. (in press).
[25]H. Sun, A. Chawathe, H. Hoteit, X. Shi, and L. Li, "Understanding shale gas production mechanisms through reservoir simulation," in *SPE/EAGE European Unconventional Resources Conference and Exhibition* (Society of Petroleum Engineers, Vienna, Austria, 2014).
[26]C. R. Clarkson, M. Nobakht, D. Kaviani, and T. Ertekin, SPE J. **17**, 230–242 (2012).
[27]T. Ertekin, G. A. King, and F. C. Schwerer, SPE Form. Eval. **1**, 43–51 (1986).
[28]F. Comets, S. Popov, G. Schütz, and M. Vachkovskaia, J. Stat. Phys. **140**, 948–984 (2010).
[29]R. F. Cracknell, D. Nicholson, and N. Quirke, Phys. Rev. Lett. **74**, 2463 (1995).
[30]S. Wang, Y. Yu, and G. Gao, Chin. J. Chem. Eng. **14**, 164–170 (2006).
[31]S.-M. Wang, Y.-X. Yu, and G.-H. Gao, J. Membr. Sci. **271**, 140–150 (2006).
[32]T. Yoshioka, M. Asaeda, and T. Tsuru, J. Membr. Sci. **293**, 81–93 (2007).
[33]H. Takaba, Y. Onumata, and S.-i. Nakao, J. Chem. Phys. **127**, 054703 (2007).
[34]K. P. Travis and K. E. Gubbins, J. Chem. Phys. **112**, 1984–1994 (2000).
[35]Z. Mao and S. B. Sinnott, J. Phys. Chem. B **104**, 4618–4624 (2000).
[36]S. K. Bhatia, O. Jepps, and D. Nicholson, J. Chem. Phys. **120**, 4472–4485 (2004).
[37]S. K. Bhatia and D. Nicholson, AIChE J. **52**, 29–38 (2006).
[38]R. Krishna and J. M. van Baten, Chem. Eng. Sci. **64**, 3159–3178 (2009).
[39]R. Krishna and J. M. van Baten, Chem. Eng. Sci. **64**, 870–882 (2009).
[40]S. K. Bhatia, M. R. Bonilla, and D. Nicholson, Phys. Chem. Chem. Phys. **13**, 15350–15383 (2011).
[41]G. Arya, H.-C. Chang, and E. J. Maginn, Mol. Simul. **29**, 697–709 (2003).
[42]G. S. Heffelfinger and F. v. Swol, J. Chem. Phys. **100**, 7548–7552 (1994).
[43]L. Xu, M. G. Sedigh, M. Sahimi, and T. T. Tsotsis, Phys. Rev. Lett. **80**, 3511 (1998).
[44]J. R. Bordin, J. S. Andrade, A. Diehl, and M. C. Barbosa, J. Chem. Phys. **140**, 194504 (2014).
[45]J. R. Bordin, A. Diehl, and M. C. Barbosa, J. Phys. Chem. B **117**, 7047–7056 (2013).
[46]M. G. Martin and J. I. Siepmann, J. Phys. Chem. B **102**, 2569–2577 (1998).
[47]W. C. Swope, H. C. Andersen, P. H. Berens, and K. R. Wilson, J. Chem. Phys. **76**, 637–649 (1982).
[48]H. J. C. Berendsen, J. P. M. Postma, W. F. van Gunsteren, A. DiNola, and J. R. Haak, J. Chem. Phys. **81**, 3684–3690 (1984).
[49]M. P. Allen and D. J. Tildesley, *Computer Simulation of Liquids* (Clarendon, Oxford, 1987).
[50]D. M. Ford and G. S. Heffelfinger, Mol. Phys. **94**, 673–683 (1998).
[51]A. Papadopoulou, E. D. Becker, M. Lupkowski, and F. van Swol, J. Chem. Phys. **98**, 4897–4908 (1993).
[52]P. Schofield, Comput. Phys. Commun. **5**, 17–23 (1973).
[53]B. Widom, J. Chem. Phys. **39**, 2808–2812 (1963).
[54]D. Frenkel and B. Smit, *Understanding Molecular Simulation, from Algorithms to Applications*, 2nd ed. (Academic Press, San Diego, London, 2001).
[55]A. Vieira-Linhares and N. Seaton, Chem. Eng. Sci. **58**, 4129–4136 (2003).
[56]M. Whitby, L. Cagnon, M. Thanou, and N. Quirke, Nano Lett. **8**, 2632–2637 (2008).
[57]W. A. Steele, Surf. Sci. **36**, 317–352 (1973).